

CrossMark
click for updatesCite this: *J. Mater. Chem. C*, 2015, 3, 632

Three-dimensional magnetite replicas of pollen particles with tailorable and predictable multimodal adhesion†

Ismael J. Gomez,†^a W. Brandon Goodwin,‡^b Dan Sabo,^c Z. John Zhang,^c Kenneth H. Sandhage*^{b,c} and J. Carson Meredith*^a

The ability to synthesize large quantities of 3-D microparticles with tunable adhesion is critically important for a variety of mature and emerging technologies, such as for paints, inks, chemical/water purification, drug delivery, cell manipulation, and assembly of hierarchical structures. Nature provides impressive examples of sustainable, complex-shaped microparticles with chemistries and structures tailored for adhesion, among the most common of which are pollen grains. We have recently used a surface sol-gel (SSG) coating process to generate iron oxide replicas of sunflower pollen grains. While these replicas exhibited multimodal adhesion, the tailorable and predictability of such adhesion was not examined. In the present paper, the layer-by-layer SSG process has been used to carefully adjust the amount of iron oxide deposited onto the pollen grains. Controlled-atmosphere thermal treatments then yielded freestanding replicas with tailored hematite (α -Fe₂O₃) or magnetite (Fe₃O₄) contents. The 3-D morphology of the starting pollen was well-preserved in the all-oxide replicas, and the shrinkage upon firing could be controlled by increasing the number of Fe–O-bearing layers deposited on the pollen. While the short-range van der Waals (VDW) adhesion of the oxide replicas to a variety of surfaces was lower than for the larger starting pollen grains, this difference was not due to shrinkage of the replicas. Analyses with a simple Hamaker model indicated that VDW adhesion of the oxide replicas was governed by the contact of oxide nanocrystals located on the spine tips (as opposed to the curvature of the entire spine tip). The longer-range attraction to a magnetic substrate could be tailored independently of the short-range VDW attraction by controlling the magnetite content of the replicas, and a simple and effective model for describing such magnetic attraction was developed. This work demonstrates that sustainable pollen microparticles can be converted into high-fidelity 3-D oxide replicas with predictable and tailorable multimodal adhesion.

Received 28th August 2014
Accepted 9th November 2014

DOI: 10.1039/c4tc01938e

www.rsc.org/MaterialsC

Introduction

The tunability of magnetic attraction is a key factor in the design of microparticles for magnetorheological fluids (*e.g.*, for

vibration damping), magnetophoretic separations, biological cell isolation and manipulation, microfluidics, targeted drug delivery, magnetic self-assembly of hierarchical structures, and the magnetic-field enabled tailoring of composite microstructures.¹ The coupling of other modes of attraction/adhesion with tunable magnetic forces could also provide new avenues for tailoring of the interactions of microparticles with surfaces.

Inspiration for the development of adhesive, structurally-complex microparticles can be found in nature. For example, diatoms (unicellular algae) and flowering plants produce silica-bearing frustules and sporopollenin-bearing pollen grains, respectively, in great quantities throughout the world and in a tremendous variety of three-dimensional (3-D) morphologies.^{2,3} The surface chemistries and morphologies of these biogenic microparticles allow for selective and strong adhesion to natural and man-made surfaces.⁴ Given their complex and diverse morphologies and sustainable (biological) production, these 3-D microparticles have attracted significant interest in recent years as templates for chemical conversion into replicas

^aGeorgia Institute of Technology, School of Chemical and Biomolecular Engineering, 311 Ferst Drive, Atlanta, GA 30332-0100, USA. E-mail: carson.meredith@chbe.gatech.edu; Tel: +1-404-385-2151

^bGeorgia Institute of Technology, School of Materials Science and Engineering, 771 Ferst Drive, Atlanta, GA 30332-0245, USA. E-mail: ken.sandhage@mse.gatech.edu; Tel: +1-404-894-6882

^cGeorgia Institute of Technology, School of Chemistry and Biochemistry, 901 Atlantic Drive, Atlanta, GA 30332-0400, USA

† Electronic supplementary information (ESI) available: Additional descriptions are provided of: (i) the method used to evaluate the diameters of uncoated pollen grains and coated pollen grains as a function of thermal treatment, and (ii) the simulation of the magnetostatic potential and magnetic field strength around the Ni–Nd substrate, along with Fig. S1–S7 and Tables S1 and S2. See DOI: 10.1039/c4tc01938e

‡ These authors contributed equally.

comprised of synthetic (non-biologically-derived) materials.⁵ We have recently reported the first generation of 3-D ferrimagnetic (Fe_3O_4) replicas of sunflower (*Helianthus annuus*) pollen grains *via* the use of a surface sol-gel (SSG) coating process.⁶ While such replicas were found to exhibit multimodal (van der Waals and magnetic) adhesion, the extent to which such adhesion could be controllably tuned and predicted was not evaluated. The objectives of this paper are: (i) to examine the tailorability of adhesion of 3-D iron oxide replicas of sunflower pollen particles to various surfaces through the use of the layer-by-layer (LbL) SSG process, and (ii) to evaluate the applicability of simple models for describing short-range and long-range attractive forces acting on such chemically-tailored, complex-shaped replicas. Such knowledge would aid in the design of complex-shaped microparticles for predictable and tailorable multimodal adhesion.

Experimental

Pollen preparation

Sunflower (*Helianthus annuus*) pollen particles were utilized as templates for conversion, *via* a coating-based process, into iron oxide (hematite, $\alpha\text{-Fe}_2\text{O}_3$, or magnetite, Fe_3O_4) replicas. Prior to coating, the pollen particles (Greer Laboratories, Lenoir, NC USA) were cleaned⁷ in order to remove the external pollenkitt coating by immersion for 24 h in a chloroform/methanol (3/1 volume ratio) solution, removed from the solution by filtration (P5 filter paper, Fisher Scientific, Pittsburgh, PA USA), and then dried at 60 °C for 12 h under vacuum. A second immersion treatment, in 1 M hydrochloric acid for 1 h, was conducted to remove residual inorganic material. The pollen grains were then rinsed three times with de-ionized water and dried by vacuum aspiration for 5 min at room temperature.

Computer-automated LbL SSG deposition

A computer-automated pumping system was used to apply Fe-O-bearing coatings to the cleaned pollen grains *via* the layer-by-layer (LbL) surface sol-gel (SSG) process.⁸ Pollen grains were first immersed with stirring in a solution of 0.0125 M $\text{Fe}(\text{III})$ isopropoxide (Alfa Aesar, Ward Hill, MA USA) in anhydrous 2-propanol (>99.8% purity, Acros Organics, Geel, Belgium) for 10 min to enable the chemisorption of a Fe-O-bearing layer. The grains were then rinsed three times with anhydrous 2-propanol (to wash away excess, non-chemisorbed alkoxide) followed by filtration under vacuum. To allow for hydrolysis of the unreacted pendant alkoxide groups on the chemisorbed Fe-O-bearing layer, the pollen particles were then immersed with stirring in de-ionized water (DIW) for 5 min. After rinsing three times with anhydrous 2-propanol, the particles underwent vacuum filtration and drying by vacuum aspiration for 5 min. To build up Fe-O-bearing coatings of varied thickness, this cyclic process (one cycle = alkoxide exposure, 2-propanol rinsing, DIW exposure, 2-propanol rinsing, drying) was conducted 10, 20, 30, 40, or 50 times.

Thermal processing

To generate freestanding polycrystalline hematite replicas of the pollen grains, the coated pollen particles were heated in air at a rate of 0.5 °C min^{-1} to a peak temperature of 600 °C, and then held at this temperature for 4 h. Conversion of the hematite pollen replicas into phase-pure magnetite was conducted *via* use of a Rhines pack comprised of a mixture of Fe (99% purity, Acros Organics) and Fe_3O_4 (99.95% purity, Alfa Aesar).⁹ Hematite pollen replicas were sealed with an excess amount of this Rhines pack powder mixture (Fe : Fe_3O_4 : Fe_2O_3 replica mole ratio = 14 : 14 : 1) inside a mild steel ampoule. The sealed ampoules were then heated at a rate of 3 °C min^{-1} to a peak temperature of 550 °C and held at this temperature for 2 h. The ampoules were then cooled to room temperature and cut open to allow for extraction of the magnetite pollen replicas.

Substrate preparation and characterization

The adhesion of cleaned sunflower pollen grains and iron oxide replicas to three types of inorganic substrates (silicon, Si; nickel, Ni; nickel-coated neodymium alloy, Ni-Nd) and three types of organic substrates (polyvinyl alcohol, PVA; polyvinyl acetate, PVAc; polystyrene, PS) was examined. The Si substrates (Silicon, Inc., Boise, ID USA) were cleaned (piranha etched) by exposure for 1 h at 80 °C to a solution comprised of 75 vol% sulfuric acid (97% purity, BDH Chemicals Ltd., Radnor, PA USA) and 25 vol% hydrogen peroxide (30 wt%, BDH Chemicals Ltd.). The Ni substrates consisted of foil (0.150 mm thickness, grade 200, 99.5% purity, Shop-aid, Inc., Woburn, MA USA) that was polished (PM5 System, Logitech Ltd., Glasgow, Scotland UK) with a suspension of colloidal silica (0.06 μm dia., Metlab Corp., Niagara Falls, NY USA). The Ni-Nd substrate was generated by attaching the polished Ni foil to an axially-poled, Nd-Fe-B alloy permanent magnet disk (ND022N-35, 5 mm diameter, 1.5 mm thick, Master Magnetics, Inc., Castle Rock, CO USA).⁶ The Nd-Fe-B disk magnet possessed a residual induction of 12 300 G. The organic substrates (PVA, PVAc, PS) consisted of polymeric films deposited by blade casting onto the silicon substrates. The solutions used for such blade casting were comprised of: 15 wt% PS (MW = 100 000, Avocado Research Chemicals, Lancashire UK) dissolved in toluene (Sigma-Aldrich, St. Louis, MO USA); 20 wt% PVAc (MW = 50 000, Alfa Aesar) dissolved in tetrahydrofuran (THF, BDH Chemicals Ltd.); or 3 wt% PVA (MW = 89 000–98 000, Sigma-Aldrich) dissolved in hexafluoro-isopropanol (HFIP, TCI America, Portland, OR USA). Blade casting was conducted (3540 Bird Film Applicator, Elcometer, Rochester Hills, MI USA) with a gap of 1.2 mm between the blade and the silicon substrate. The cast films were allowed to dry for 2 days at 23 °C in a saturated solvent (toluene, THF, or HFIP) environment, and then for 2 more days at 23 °C in air. The films were then annealed in a vacuum oven for 1 day at 100 °C. The resulting polymeric films completely covered the silicon substrate and possessed average thicknesses of 20–100 μm .

The roughness of each type of substrate was determined by scanning probe microscopy (Dimension 3100 SPM equipped with a Nanoscope V Controller, Veeco Instruments, Inc., Plainview, NY USA) using a pyramidal tip silicon cantilever

(Applied NanoStructures, Inc., Santa Clara, CA USA) operated in tapping mode (200–400 kHz). Three randomly-located scans over a total area of $100 \mu\text{m}^2$ ($10 \mu\text{m} \times 10 \mu\text{m}$) were conducted for each substrate, with each scan area divided into 4 sectors. An average roughness value (R_a , in nm) for a given substrate was obtained from analysis of these 12 sectors.

Pollen and pollen replica characterization

Secondary electron (SE) images and chemical analyses of cleaned sunflower pollen and oxide replicas were obtained with a field emission gun instrument (Carl Zeiss SMT, Ltd., Thornwood, NY USA) equipped with an energy dispersive X-ray spectrometer (INCA EDS, Oxford Instruments, Abingdon, Oxfordshire UK). The diameters of native pollen and oxide pollen replica particles were obtained by fitting a circle around the pollen grain spines (echini) and measuring the diameter of the circle. Changes in diameter upon thermal treatment were obtained from measurements of the same coated or uncoated pollen grain before and after such treatment (see Fig. S1 and S2†), with at least three such before/after pairs of measurements conducted to obtain average values. Average values of the spine tip radii of native pollen and oxide pollen replicas were obtained from SE images of individual particles attached to cantilever probes (described below). For each such particle/cantilever probe assembly, the average value of the radius of curvature was obtained for five spine tips positioned closest to the location where the particle made contact to the substrate.

The crystalline phase content and average crystal size of the oxide pollen replicas were evaluated by X-ray diffraction (XRD) analyses conducted with Cu $K\alpha$ radiation using a diffractometer (X-Pert Pro Alpha 1, PANalytical, Almelo, The Netherlands) equipped with an incident beam Johannsen monochromator (PANalytical) and an Xcelerator linear detector (PANalytical). The average crystallite size was determined by applying the profile fit function of JADE software (Materials Data, Inc., Livermore, CA) to obtain values of the diffraction peak width, at half of the maximum peak intensity, for input into Scherrer's formula.

Thermogravimetric (TG) analyses were used to evaluate the mass change upon heating of coated (10–50 SSG cycles) pollen grains at a rate of $5 \text{ }^\circ\text{C min}^{-1}$ in flowing (50 ml min^{-1}) synthetic (20% O_2 , 80% N_2) air. A similar starting sample batch weight of $\sim 0.5 \text{ g}$ was used for all TG analyses.

The magnetization hysteresis behaviour of Fe_3O_4 replicas of sunflower pollen particles was examined at 300 K at applied magnetic fields of up to 5 T using a superconducting quantum interference device (SQUID) magnetometer (Quantum Design MPMS-5S, San Diego, CA USA).

Adhesion and magnetic force measurements

Adhesion measurements were conducted using probes consisting of a single pollen particle or a single oxide replica particle attached to a tipless silicon atomic force microscope (AFM) cantilever (FORT-TL, Applied NanoStructures, Inc.) using a procedure described previously.⁶ For the cleaned pollen and for each type of oxide replica particle (*i.e.*, Fe_2O_3 or Fe_3O_4

replicas prepared with 10, 20, 30, 40, or 50 SSG cycles), three single-particle-bearing cantilever probes were prepared (for a total of 33 particle/cantilever probes). Adhesion force measurements were evaluated with a scanning probe microscope (Dimension 3100 SPM equipped with a Nanoscope V Controller, Veeco Instruments, Inc., Plainview, NY USA) operated in contact mode at room temperature in the ambient atmosphere (note: the relative humidity in the laboratory during these adhesion measurements ranged from 30 to 35%). The spring constants, determined with the scanning probe microscope, of the different particle/cantilever probes (sunflower pollen-bearing, Fe_2O_3 replica-bearing, or Fe_3O_4 replica-bearing) are listed in Table 1. Contact adhesion measurements were conducted using a constant load force of 2.5 nN. For each particle/cantilever probe and substrate, 20 separate contact adhesion measurements at different locations on the substrate surface were conducted to obtain plots of the force *vs.* vertical distance from the substrate. A total of 60 measurements were obtained for each type of particle/cantilever probe (20 measurements \times 3 probes of the same type). The depth of adhesion wells obtained upon retraction for these 60 measurements were averaged. Statistical analyses to evaluate the significance of differences between adhesion data sets were conducted using *t*-tests (with $\alpha = 0.05$). Unless otherwise noted, the error bars presented in this study reveal a range of ± 1 standard deviation.

The magnetic force acting on a given Fe_3O_4 replica of a pollen particle was obtained with the use of the Ni foil-coated, axially-poled Nd–Fe–B alloy disk (Ni–Nd) substrate. Prior to each particular Fe_3O_4 particle/cantilever probe test, the probe was first positioned at a fixed distance of $140 \mu\text{m}$ above the Ni–Nd substrate surface and then scanned sideways across the substrate to identify the lateral position at which the magnetic force was strongest. This lateral location ($\sim 300 \mu\text{m}$ from the outer edge of the disk-shaped Ni–Nd substrate) was then used to evaluate the change in magnetic force with vertical distance from the Ni–Nd surface. For each particular Fe_3O_4 particle/cantilever probe, 20 separate force-vertical distance scans were obtained. Force-vertical distance scans were also obtained using a $10.4 \mu\text{m}$ diameter ferromagnetic CrO_2 -coated polystyrene (CrO_2 -PS) microsphere ($M_r = 6.3 \text{ emu g}^{-1}$, 20 vol% CrO_2 , Spherotech, Inc., Lake Forest, IL USA) attached to a tipless cantilever.

Theory

The force acting on a magnetic particle (F_m) interacting with a magnetic field gradient associated with a permanent magnet may be expressed as:¹⁰

$$F_m = \mu_0 V_m M \nabla H \quad (1)$$

where μ_0 ($4\pi \times 10^{-7} \text{ N A}^{-2}$) is the permeability of free space, V_m (m^3 per particle) is the solid volume of magnetic material within the particle, M (A m^{-1}) is the magnetization, and ∇H (A m^{-2}) is the gradient in the magnetic field strength. Because the Fe_3O_4 sunflower replicas were anchored to tipless cantilevers, the

Table 1 Measured values of the cantilever probe spring constant (N m^{-1})

SSG cycles:	0	10	20	30	40	50
Cleaned	1.84–2.34	—	—	—	—	—
Fe_2O_3	—	1.44–2.26	1.08–1.66	1.19–1.91	0.81–1.53	1.60–3.10
Fe_3O_4	—	1.92–2.30	1.15–2.05	1.63–1.69	0.91–1.67	1.37–1.61

direction of particle motion was restricted to the direction of cantilever deflection (herein referred to as the z direction). Therefore, the magnetic force acting on the Fe_3O_4 particle/cantilever assembly interacting with the permanent magnet can be expressed as:

$$F_m = \mu_0 V_m M \frac{\partial H}{\partial z} \hat{z} \quad (2)$$

where $\partial H/\partial z$ is the gradient of the magnetic field in the z -direction and \hat{z} is the unit vector parallel to the z direction. In order to utilize eqn (2), $\partial H/\partial z$ needed to be evaluated.

The spatial dependence of the magnetostatic potential, Φ (A), of a disk-shaped permanent magnet may be expressed in cylindrical coordinates as:¹¹

$$\nabla^2 \Phi = \frac{\partial^2 \Phi}{\partial r^2} + \frac{1}{r} \frac{\partial \Phi}{\partial r} + \frac{\partial^2 \Phi}{\partial z^2} = 0 \quad (3)$$

where Φ and H are related by:

$$H = -\nabla \Phi \quad (4)$$

The magnetostatic potential and magnetic field associated with the Ni–Nd disk-shaped substrate were modeled by applying a finite difference approach described elsewhere¹¹ to eqn (3) and (4). The finite difference model was coded in FORTRAN77 and numerically evaluated using NAG Fortran Builder 5.2 software. This simulation was conducted using a $50 \text{ mm} \times 50 \text{ mm}$ grid and a $50 \mu\text{m}$ step size for the disk-shaped Ni–Nd substrate of 1.5 mm diameter and 5 mm thickness. Values of $\partial H/\partial z$ were then calculated for use with eqn (2).

Results and discussion

Pollen conversion into freestanding 3-D magnetic replicas

The repeated, alternating exposure of sunflower pollen particles to a propanolic solution of iron alkoxide and water was examined as a means of controllably applying Fe–O-bearing layers that, upon subsequent thermal treatment, could be converted into freestanding iron oxide replicas. Prior work has shown that such a LbL SSG process can be used to deposit highly-conformal coatings onto complex 3-D templates, provided that the substrate possesses (or has been functionalized so as to possess) a high density of surface hydroxyl groups.⁸ While the sporopollenin comprising the exine (outer layer) of pollen particles has been reported to contain significant amounts of dicarboxylic and/or fatty acids,¹² direct measurements of the density and spatial distribution of such OH-bearing molecules across the exine surface have not been reported. Because the chemisorption of iron alkoxide molecules to the pollen surface

requires reaction with surface hydroxyl groups,¹³ the SSG process provides an indirect means of evaluating the surface –OH density/distribution. Secondary electron (SE) images of sunflower pollen particles after exposure to 10 or 50 SSG deposition cycles are shown in Fig. 1a and b, respectively, with higher magnification images of the surfaces of a cleaned pollen particle and a coated particle presented in Fig. S3a and b.[†] The roughly spherical shape and the sharp echini (spines) and other surface features (*e.g.*, pores present at the base of the echini) in the uncoated pollen particles were retained in the 10 and 50 SSG cycle samples, and significant gaps in the Fe–O-bearing coating

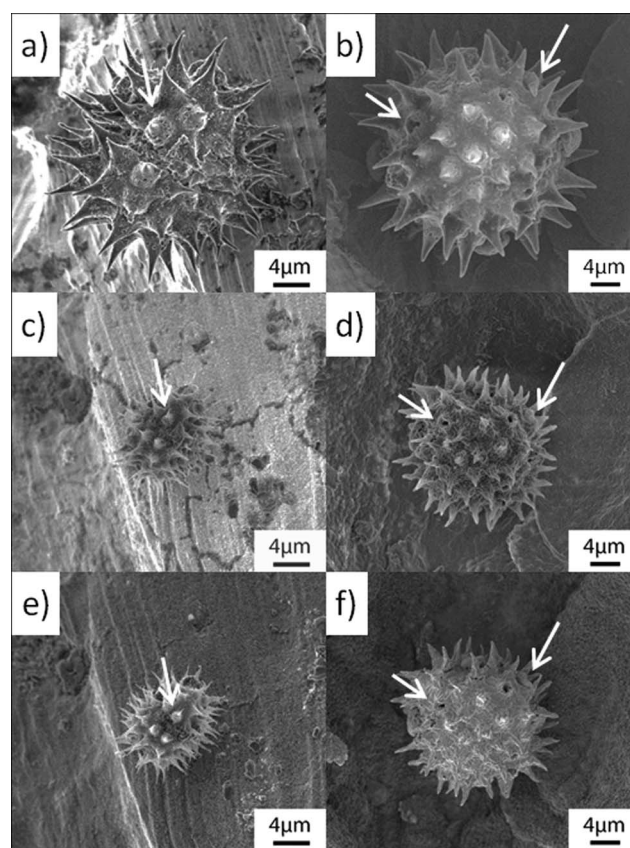


Fig. 1 SE images of sunflower pollen particles at various stages of conversion into Fe_3O_4 : (a), (b) Fe–O-coated grains after 10 and 50 SSG deposition cycles, respectively; (c), (d) Fe_2O_3 replicas of the same grains shown in (a) and (b), respectively, after pyrolysis at a peak temperature of $600 \text{ }^\circ\text{C}$ for 4 h in air, and (e), (f) Fe_3O_4 replicas of the same Fe_2O_3 grains shown in (c) and (d), respectively, generated by partial reduction using a Rhines pack mixture ($\text{Fe}/\text{Fe}_3\text{O}_4$) at $550 \text{ }^\circ\text{C}$ for 2 h. The white arrows reveal features retained on the same particles at various stages of conversion from (a) to (c) to (e) or from (b) to (d) to (f).

were not detected. Such conformal coatings were consistent with the presence of a high and uniform concentration of hydroxyl groups on the sunflower pollen grain surface.

Conversion of Fe–O-coated pollen particles into freestanding (sporopollenin-free) polycrystalline Fe_2O_3 was accomplished *via* organic pyrolysis and oxide crystallization upon heating to 600 °C in air. Dynamic TG analyses (Fig. 2a) indicated that such pyrolysis was completed within a few minutes after reaching the peak temperature of 600 °C. The relative amount of oxide present after complete organic pyrolysis was found to increase monotonically with the number of alkoxide/water deposition cycles applied to the pollen grains (Fig. 2b), which was consistent with a gradual build up in the amount of iron oxide deposited on the pollen during the LbL SSG process. XRD analyses (Fig. 3a) confirmed the presence of phase-pure hematite ($\alpha\text{-Fe}_2\text{O}_3$) in the pollen replicas after the 600 °C/4 h treatment in air, with Scherrer analyses yielding an average crystallite size of 35–39 nm (Fig. 3c). SE images (Fig. 1c and d) revealed that the 3-D morphology of the sunflower pollen grains was retained by these Fe_2O_3 -converted specimens. Such shape preservation in the freestanding Fe_2O_3 replicas provided confirmation of the conformality and continuity of the SSG deposited Fe–O layers (note: pollen grains exposed to only 2 SSG deposition cycles could, upon organic pyrolysis, be converted into freestanding, albeit fragile, replicas, as shown in Fig. S8†). While the Fe_2O_3 replicas were noticeably smaller than the starting pollen grains (Fig. 1), the extent of shrinkage upon

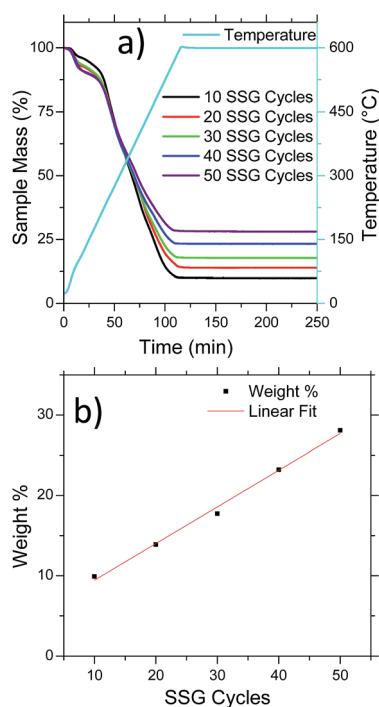


Fig. 2 TG analyses of Fe–O coated sunflower pollen particles (10–50 SSG deposition cycles) during pyrolysis upon heating to 600 °C in flowing synthetic (20% O_2 /80% N_2) air. The influence of the number of SSG cycles on the weight change with temperature, and on the relative retained weight after complete pyrolysis, are shown in (a) and (b), respectively.

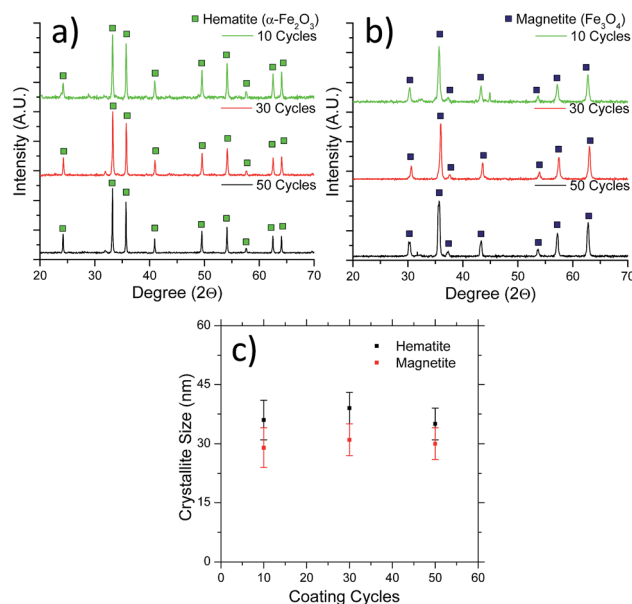


Fig. 3 XRD analyses of iron oxide replicas of pollen grains generated by exposing sunflower pollen particles to 10, 30, and 50 SSG deposition cycles followed by: (a) heating to a peak temperature of 600 °C for 4 h in air for conversion into hematite ($\alpha\text{-Fe}_2\text{O}_3$) replicas, and then (b) heating in a sealed iron ampoule along with a Fe/ Fe_3O_4 Rhines pack mixture to 550 °C for 2 h for conversion into magnetite (Fe_3O_4) replicas. (c) Average values of crystallite size for these hematite and magnetite samples, as determined from Scherrer XRD analyses.

firing was found to decrease monotonically with an increase in the number of deposited Fe–O layers (Fig. 4).

To further evaluate such thermally-induced shrinkage and oxide crystallization, uncoated pollen grains and pollen grains coated with 50 SSG layers were heated in air at a constant rate of 0.5 °C min to a peak temperature in the range of 200 °C to 600 °C, and then held at this peak temperature for 4 h. The change in average diameter of an uncoated or coated pollen

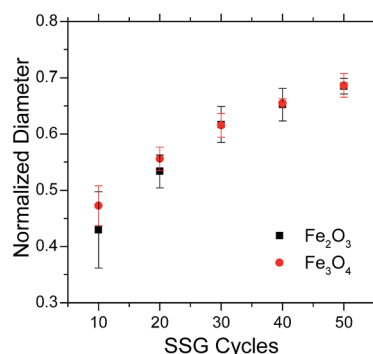


Fig. 4 Shrinkage of Fe–O-coated pollen grains, after pyrolysis at 600 °C for 4 h in air, as a function of the number of applied SSG deposition cycles. The normalized diameter is the ratio of the oxide pollen grain replica diameter to the diameter of the same grain prior to firing (with the diameter measured in each case from a spine tip on one side to a spine tip on the opposite side of a given pollen grain or pollen grain replica).

grain was then determined from SE images of the same particle before and after such a thermal treatment. As shown in Fig. 5 and S4a–h,† the uncoated pollen grains exhibited a monotonic decrease in size with increasing temperature, with complete pyrolysis occurring within 4 h at 600 °C (as expected from TG analyses). However, the change in diameter of the pollen grains coated with 50 SSG layers was the same after all of the thermal treatments examined (Fig. 5 and S5a–h†). In other words, the shrinkage of the pollen grains coated with 50 SSG layers was completed even after the 200 °C/4 h treatment, which was well before the underlying organic template had been completely burned away.

Interestingly, XRD analyses of the pollen grains with 50 SSG layers (Fig. S6†) revealed little crystallization after the 200 °C/4 h treatment, whereas extensive hematite crystallization was detected after the 300 °C/4 h and higher temperature treatments. Apparently, the 50 layer Fe–O-bearing coating became sufficiently rigid during the 200 °C/4 h, without the need for extensive hematite crystallization, as to avoid further shrinkage.

The conversion of hematite pollen replicas into phase-pure magnetite replicas was conducted *via* use of a controlled oxygen partial pressure heat treatment using a Rhines pack⁹ mixture of Fe and Fe₃O₄; that is, the hematite pollen replicas were sealed, along with an excess mixture of iron and magnetite powder, inside a mild steel ampoule. At temperatures below 570 °C, wustite (Fe_{1–x}O) is thermodynamically unstable at ambient pressure,¹⁴ so that iron and magnetite can coexist at equilibrium at ≤550 °C. Upon heating to 550 °C, the oxygen partial pressure established by the excess Fe/Fe₃O₄ mixture can result in the reduction of Fe₂O₃ into Fe₃O₄ (*i.e.*, *via* oxidation of some of the Fe in the Rhines pack into Fe₃O₄). Complete conversion of the hematite pollen replicas into magnetite was accomplished within 4 h at 550 °C, as confirmed by XRD analysis (Fig. 3b). The average crystallite size of the magnetite-converted pollen grains (Fig. 3c) was in the range of 29–31 nm. SE images of the magnetite-converted grains (Fig. 1e and f) indicated that these specimens retained the 3-D morphologies and surface features of the starting pollen and hematite pollen replicas. The calculated change in solid volume associated with the conversion of dense hematite into dense magnetite is small (–2.0% (ref. 15)).

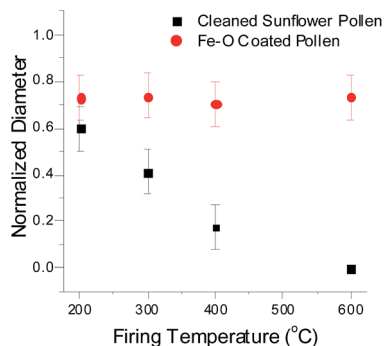


Fig. 5 Shrinkage of a cleaned sunflower pollen grain and a Fe–O-coated (50 SSG cycles) pollen grain as a function of thermal treatment in air for 4 h at the indicated temperature.

Indeed, for specimens coated with 30 or more SSG deposition cycles, measurements of the diameters of the magnetite replica grains revealed no detectable change relative to the same grains (as hematite) prior to the partial reduction thermal treatment (Fig. 4). However, as the number of SSG coating cycles decreased to 20 and 10, a small decrease in the value of the average diameter was detected, which may have been a result of the susceptibility of such thinly-coated specimens to some additional particle shrinkage during the second 550 °C/2 h (Rhines pack) thermal treatment.

The magnetic hysteresis behaviour of Fe₃O₄ replicas generated with the use of 10 and 50 SSG deposition cycles was examined with a SQUID magnetometer at 300 K. As shown in Fig. 6, distinct magnetic hysteresis loops, consistent with ferrimagnetic materials, were obtained for both samples. The values of coercive field (H_c) for the 10 and 50 SSG cycle samples were $1.52 \times 10^4 \text{ A m}^{-1}$ (0.019 T) and $1.37 \times 10^4 \text{ A m}^{-1}$ (0.017 T), respectively, which were similar to values reported by several authors for thin, polycrystalline magnetite films with average crystal sizes of 40–50 nm.¹⁶ Such modest values of H_c allowed for ready alignment of magnetic domains in these specimens upon exposure to the magnetic field present near the edge of the Ni–Nd substrate. Indeed, the magnetization values achieved with these Fe₃O₄ pollen replicas for the magnetic field strength encountered near the edge of the Ni–Nd magnetic substrate (about 0.38 T) were not far from the saturation magnetization values shown in Fig. 6.

Adhesion of pollen and pollen replicas

The adhesion of cleaned sunflower pollen and oxide pollen replicas (Fe₂O₃ and Fe₃O₄ replicas generated with the use of 10–50 SSG deposition cycles) to various substrates was evaluated with the use of single-particle-bearing AFM cantilever probes of the type shown in Fig. 7 and Fig. S7.† Flat substrates (AFM-determined values of average roughness, $R_a \leq 2.8 \text{ nm}$, as shown in Table S1†) with a range of characteristics were selected. PVA and PVAc were chosen as proton-donor and proton-accepter substrates, respectively, whereas PS was selected as an apolar hydrocarbon substrate. Piranha solution treatment of a polished Si wafer was used to generate a thin hydroxylated silica layer to act as a hydrophilic surface.¹⁷ Polished polycrystalline

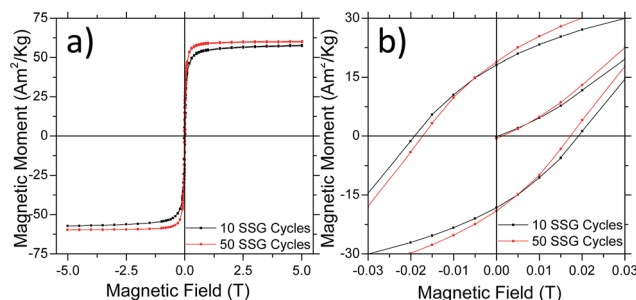


Fig. 6 Magnetic hysteresis plots obtained at 300 K for Fe₃O₄ sunflower pollen replicas synthesized with the use of 10 and 50 SSG deposition cycles.

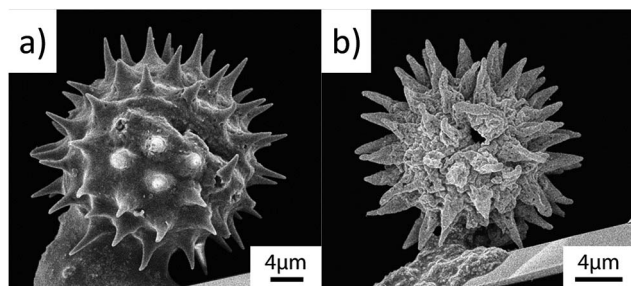


Fig. 7 Representative SE images of single-particle-bearing cantilever probes. The probes shown in (a) and (b) contained cleaned sunflower pollen and Fe_3O_4 pollen replicas (generated using 40 SSG deposition cycles), respectively.

nickel foil was used as a conductive substrate, whereas the nickel-foil-coated, axially-poled neodymium iron boron magnet (Ni–Nd substrate) was used as a strongly-magnetized substrate.

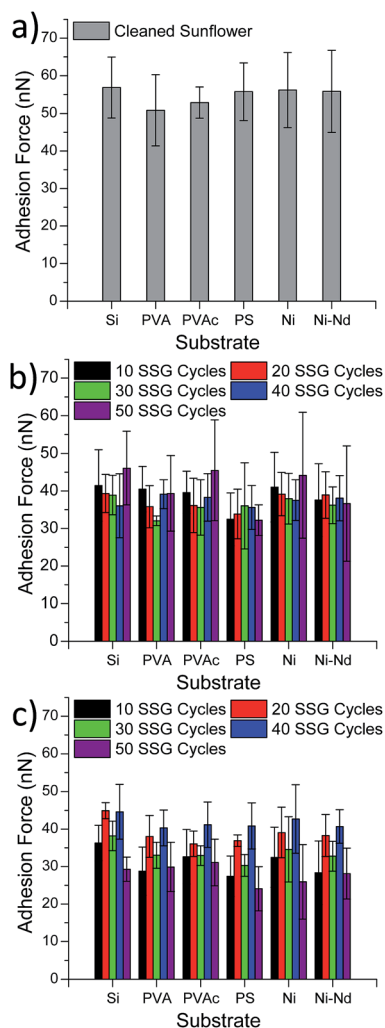


Fig. 8 AFM contact adhesion analyses of short-range VDW forces for: (a) cleaned sunflower pollen, (b) Fe_2O_3 sunflower pollen replicas (10–50 SSG deposition cycles), and (c) Fe_3O_4 sunflower pollen replicas (10–50 SSG deposition cycles) with various substrates.

Contact-mode AFM measurements of the adhesion forces of cleaned sunflower pollen and hematite and magnetite pollen replicas are presented in Fig. 8. *t*-Test analyses indicated that there was no significant statistical difference in the average short-range, contact-mode adhesion force detected for the same type of particle (cleaned sunflower, hematite replica, or magnetite replica) on the different substrates. The similarity in short-range adhesion force values for a given type of particle with the electrically-conductive substrates (Ni, Ni–Nd) and the semi-conductive/non-conductive substrates (Si, PVA, PVAc, PS) suggests that such adhesion was not strongly influenced by sustained electrostatic attraction. The similarity in short-range adhesion force values for a given type of particle with the proton-donating and proton-accepting polymeric substrates (PVA, PVAc), the hydroxylated substrate (Si), and the metallic substrates (Ni, Ni–Nd) suggests that such adhesion was also not strongly influenced by hydrogen bonding. The contact-mode adhesion force data for all of the substrates for each type of particle was then combined to obtain the overall average values shown in Table 2. The average contact-mode adhesion force values of oxide pollen replicas (28–42 nN) were significantly smaller from the average value for the cleaned sunflower pollen (55 nN). However, no significant differences were detected in the contact-mode adhesion force values with the number of SSG deposition cycles (as confirmed by *t*-test analyses) for the hematite and magnetite replicas.

An additional, significant (magnetic) force of attraction was detected between the ferrimagnetic Fe_3O_4 sunflower pollen replicas and the Ni–Nd substrate, particularly near the perimeter of this disk-shaped substrate where the magnetic field gradient was greatest (as discussed below). This force persisted out to a Fe_3O_4 particle/Ni–Nd substrate separation distance as far as ~ 1.5 mm. Such a force of attraction was not detected between the Ni–Nd substrate and the cleaned sunflower pollen or hematite pollen replicas. The total (short + long range) adhesion force acting between a given Fe_3O_4 replica particle and the Ni–Nd substrate is plotted against the distance from this substrate in Fig. 9. (Note: such force-distance measurements were conducted ~ 300 μm from the outer edge of the disk-shaped Ni–Nd substrate, where the magnetic field strength was measured to be at a maximum). For each Fe_3O_4 particle/Ni–Nd substrate pairing, the total attractive force (~ 50 – 90 nN) was comprised of a short-range (contact mode) contribution (35 ± 14 nN) and a longer-range magnetic contribution. The magnitude of this magnetic force increased monotonically with the number of SSG deposition cycles used to generate these replicas, as shown in Fig. 10.

Table 2 Contact-mode adhesion force values (in nN), averaged overall of the substrates examined, for the cleaned sunflower pollen, hematite pollen replicas, and magnetite pollen replicas

SSG cycles:	0	10	20	30	40	50
Cleaned sunflower	55 ± 9	—	—	—	—	—
Hematite	—	39 ± 9	37 ± 6	36 ± 7	38 ± 6	41 ± 13
Magnetite	—	31 ± 8	39 ± 5	34 ± 7	42 ± 7	28 ± 7

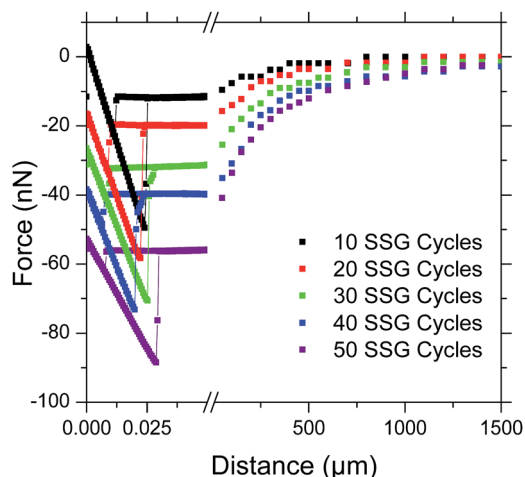


Fig. 9 Total adhesion force as a function of distance between Fe_3O_4 sunflower pollen replicas (prepared with 10–50 SSG cycles) and the Ni–Nd substrate (near the perimeter of this disk-shaped magnetic substrate).

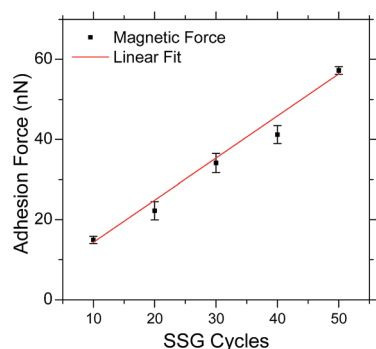


Fig. 10 Magnetic force measurements of Fe_3O_4 sunflower replicas as a function of the number of SSG deposition cycles used to prepare the replicas. The error bars indicate the 95% confidence limit range.

Control over the amount of magnetite present in the replicas, enabled by the LbL nature of the SSG process, provided a means for tuning the magnetic and, hence, total attraction of such Fe_3O_4 pollen replicas to magnetic substrates. As shown in Fig. 11, the total force of adhesion of the Fe_3O_4 replicas to the Ni–Nd substrate could be increased by a factor of ~ 1.9 by increasing the number of SSG deposition cycles from 10 to 50. Indeed, while the magnitude of the short-range, contact-mode adhesion of the magnetite pollen replicas in the absence of an applied magnetic field (*i.e.*, for adhesion to the non-magnetic PVA, PVAc, PS, Si, and Ni substrates) was smaller than for the cleaned sunflower pollen particles (Fig. 8), the total (short + long range) force of attraction of the Fe_3O_4 replicas to the Ni–Nd substrate could be tailored (by adjusting the number of SSG deposition cycles) to exceed that for the cleaned sunflower pollen particles (*e.g.*, by a factor of ~ 1.6 for 50 SSG cycles, as shown in Fig. 11).

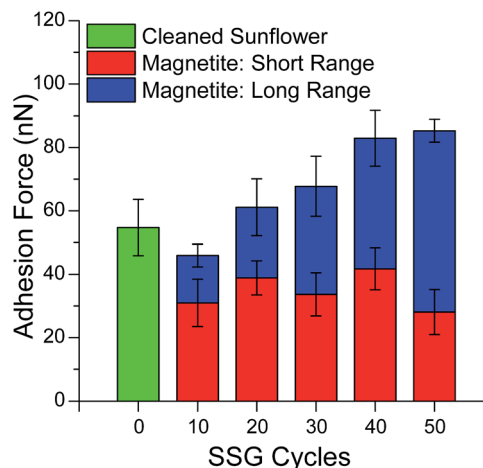


Fig. 11 Total (short + long range) force of attraction of cleaned sunflower pollen and Fe_3O_4 sunflower pollen replicas as a function of the number of SSG deposition cycles used to prepare the latter replicas.

Modelling of short-range (VDW) attraction

The short-range, contact-mode adhesion of sunflower pollen and oxide pollen replicas was evaluated with the use of a simple Hamaker model of the van der Waals (VDW) force between a sphere and a flat plane:¹⁸

$$F_{\text{VDW}} = \frac{A_{132}R}{6D^2} \quad (5)$$

where A_{132} is the non-retarded Hamaker constant of material 1 and 2 interacting across a medium 3 (air in the present case), R is the contact radius, and D is the cutoff separation distance for the VDW interaction (≈ 0.165 nm).¹⁹ Eqn (5) was used by approximating the curvatures of contacting surfaces of cleaned sunflower pollen and pollen replicas as being spherical. Lifshitz theory was used to calculate A_{132} values for Fe_2O_3 and Fe_3O_4 :¹⁹

$$A_{132} \approx \frac{3}{4}kT \left(\frac{\varepsilon_1 - \varepsilon_3}{\varepsilon_1 + \varepsilon_3} \right) \left(\frac{\varepsilon_2 - \varepsilon_3}{\varepsilon_2 + \varepsilon_3} \right) + \frac{3h\nu_e}{8\sqrt{2}} \frac{(n_1^2 - n_3^2)(n_2^2 - n_3^2)}{(n_1^2 + n_3^2)^{1/2}(n_2^2 + n_3^2)^{1/2} \{ (n_1^2 + n_3^2)^{1/2} + (n_2^2 + n_3^2)^{1/2} \}} \quad (6)$$

where k is Boltzmann's constant, T is temperature, h is Planck's constant, ν_e is the absorption frequency of all three media, ε_1 and ε_2 are dielectric constants, and n_1 and n_2 are refractive indices. A_{132} values for various coating layers of hematite or magnetite replicas on all substrates were calculated from eqn (6) by using appropriate ε_1 , ε_2 , n_1 , and n_2 values,²⁰ with the assumption that the absorption frequencies of all media were the same. By inserting the AFM-measured (average) values of contact-mode adhesion force into eqn (5) along with the calculated A_{132} constants, values of average contact radii, R , for the cleaned sunflower pollen and hematite and magnetite pollen replicas could be obtained. The value obtained for a given pollen grain or pollen grain replica could then be compared with direct measurement (*via* electron microscopy) of

the average radius of curvature of those spine tips positioned closest to the location where the particle made contact to the substrate. For cleaned sunflower pollen grains, the average values of adhesion-derived contact radii (93 ± 16 nm) and microscopy-derived spine tip radii (120 ± 12 nm) were in reasonable agreement. However, the average values of adhesion-derived contact radii of the hematite and magnetite pollen replicas (28 ± 8 nm and 26 ± 8 nm, respectively) were appreciably smaller than the average measured values of the spine tip radii for those replicas (105 ± 8 nm and 97 ± 8 nm, respectively), as shown in Fig. 12. (Note: statistical *t*-test analyses indicated that the change in calculated contact radii with the number of SSG deposition cycles was not significant for the hematite or magnetite pollen replicas). The adhesion-derived contact radii were, instead, not far from the average values of the hematite and magnetite crystal radii (19 ± 2 nm and 15 ± 2 nm, respectively) obtained from Scherrer XRD analyses. This similarity suggests that VDW adhesion of the polycrystalline oxide replicas was governed by the curvature of one or a few oxide nanocrystals present on a spine tip, instead of by the curvature of the entire spine tip.

Modelling of long-range (magnetic) attraction

Using a previously described methodology,¹¹ the space around the Ni–Nd substrate was discretized and Φ and H were simulated using eqn (3) and (4) with appropriate boundary conditions, as detailed in the ESI section.† The simulated variations in the magnetostatic potential, Φ , and magnetic field strength, H , around the magnetic Ni–Nd substrate are presented in Fig. 13a and b. The gradient in magnetic field strength, $\partial H/\partial z$, was then determined as a function of position. In order to validate this simulation, a CrO_2 -PS sphere with a known magnetization hysteresis curve and known volume of magnetic material (V_m) was attached to a tipless AFM cantilever (Fig. 14a). This CrO_2 -PS sphere/cantilever probe was positioned 140 μm above the surface of the Ni–Nd substrate and then scanned across the substrate to identify the lateral location at which the magnetic field gradient, $\partial H/\partial z$, and magnetic force, F_m , were strongest

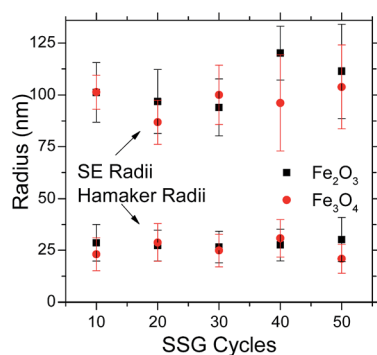


Fig. 12 Average values of the calculated contact radii from the Hamaker model ("Hamaker radii") and the measured spine tip radii from SE analyses ("SE radii") for the hematite and magnetite sunflower pollen replicas (prepared with 10–50 SSG cycles).

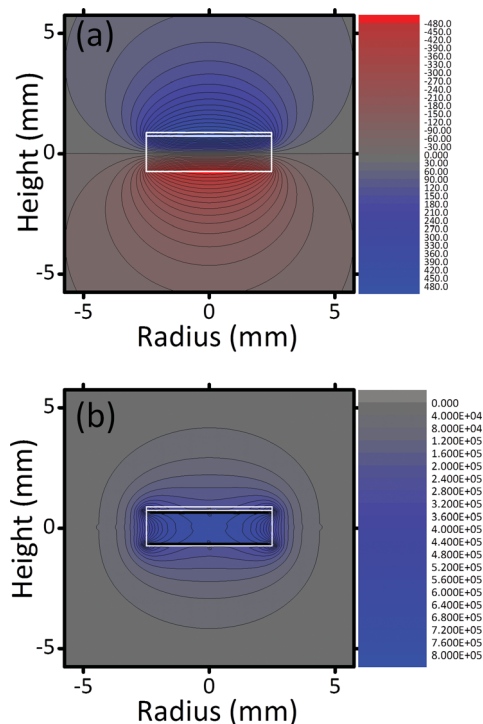


Fig. 13 Simulations of: (a) the magnetostatic potential (Φ , A) and (b) magnetic field (H , A m^{-1}) around a cross-section of the Ni–Nd substrate. The perimeters of the Nd–Fe–B magnet and attached Ni foil are highlighted in white.

(~ 300 μm from the outer edge of the disk-shaped Ni–Nd substrate). The magnetic force for this CrO_2 -PS sphere/cantilever probe at this location was then measured as a

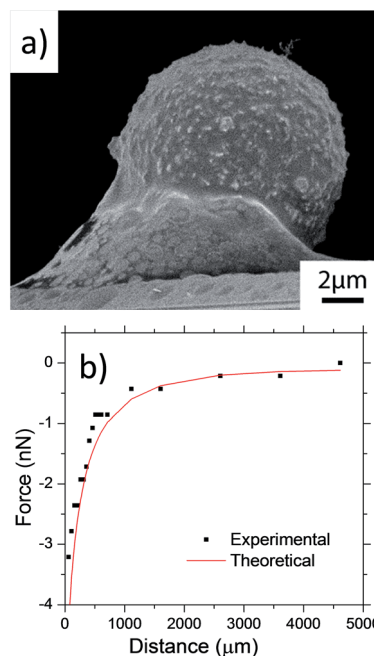


Fig. 14 (a) SE image of a CrO_2 -PS microsphere attached to a tipless AFM cantilever. (b) Comparison of the experimentally-measured and calculated magnetic force as a function of distance from the magnetic Ni–Nd substrate.

function of vertical distance from the Ni–Nd substrate. These measurements were compared to the force-distance curve calculated using eqn (2) with simulated $\partial H/\partial z$ values. As shown in Fig. 14b, good agreement was obtained between the measured and simulated magnetic force-distance curves. Armed with a validated simulation for the position dependence of $\partial H/\partial z$, measurement of the magnetic force-distance behavior of a given magnetite pollen replica could be used, along with knowledge of the magnetization, M (from the data in Fig. 6), to calculate the volume of magnetite, V_m , present within the replica *via* eqn (2). Each force measurement obtained at a given distance from the Ni–Nd substrate for a particular Fe_3O_4 pollen replica was used to obtain a V_m value. The V_m values obtained over a range of distances for a given Fe_3O_4 pollen replica were then used to obtain an average V_m value for that replica (note: a representative list of V_m values obtained from force measurements over a range of distances for a particular Fe_3O_4 pollen replica is presented in Table S2†). The average magnetic volumes determined in this manner for the Fe_3O_4 replicas are shown in Fig. 15a. A monotonic, linear increase in the calculated volume of magnetite with the number of SSG deposition cycles was observed. This trend was consistent with the layer-by-layer nature of the SSG process, as had been independently confirmed by TG analyses (Fig. 2). These average V_m values were re-inserted into eqn (2) to obtain the F_m *vs.* distance curves shown along with the data in Fig. 15b.

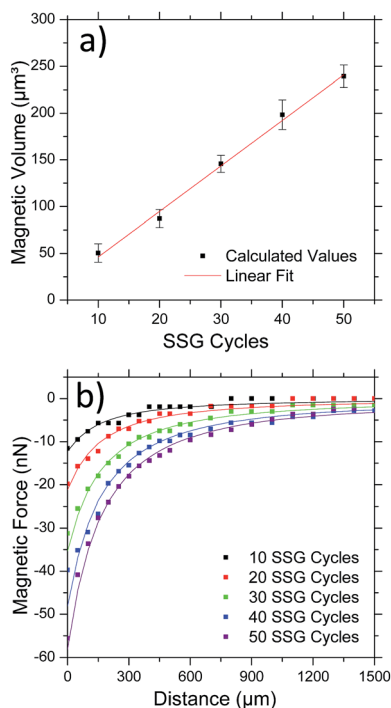


Fig. 15 (a) The calculated volume of magnetite, V_m , in a given particle obtained from the magnetic force measurements, simulation of $\partial H/\partial z$ *vs.* distance, magnetization data in Fig. 6, and use of eqn (2). These V_m values were re-inserted into eqn (2) to obtain the F_m *vs.* distance curves shown with the measured data points in (b).

Conclusions

This work demonstrates that: (i) hematite ($\alpha\text{-Fe}_2\text{O}_3$) and magnetite (Fe_3O_4) replicas of 3-D sustainable, biologically-formed organic microtemplates (sunflower pollen particles) with tailorable oxide contents can be generated using a scalable, highly-conformal wet chemical coating process, (ii) simple expressions may be used to model and predict the short-range VDW adhesion of such Fe_2O_3 and Fe_3O_4 replicas (to a variety of surfaces) and the longer-range magnetic attraction of Fe_3O_4 replicas (to magnetic surfaces), and (iii) the attraction of 3-D Fe_3O_4 replicas to magnetic surfaces can be tailored *via* proper control of this coating/thermal treatment process.

The generation of inorganic replicas of 3-D sunflower pollen microparticles comprised of controlled amounts of hematite or magnetite has been accomplished *via* a surface sol-gel (SSG) deposition process followed by thermal treatment(s) at controlled oxygen partial pressure(s). Alternating exposure of the pollen microparticles to a propanolic solution of iron(III) isopropoxide and then to water was conducted 10–50 times with a computer-automated pumping system. The layer-by-layer (LbL) nature of the deposition process was confirmed by thermogravimetric analyses, which revealed a monotonic increase in the iron oxide content of the pollen particles with an increasing number of alkoxide/water cycles. After complete organic pyrolysis upon heating to 600 °C in air, particles comprised of nanocrystalline hematite were produced that retained the 3-D shapes of, but smaller sizes than, the starting pollen grains. The extent of shrinkage upon firing could be controlled, however, by adjusting the thickness of the deposited coating; that is, the pyrolysis-induced reduction in diameter of the Fe_2O_3 replicas decreased as the number of deposited SSG layers increased. The Fe_2O_3 replicas were fully converted into Fe_3O_4 replicas of similar size by partial reduction at 550 °C at an oxygen partial pressure established by the $\text{Fe}_3\text{O}_4/\text{Fe}$ equilibrium (*via* use of a $\text{Fe}_3\text{O}_4/\text{Fe}$ Rhines pack).

Values of the short-range van der Waals (VDW) adhesion force obtained for the hematite and magnetite pollen replicas on a variety of flat organic and inorganic substrates (with non-retarded Hamaker constants ranging from 1.7–3.4) were smaller than for larger cleaned sunflower pollen particles. However, such a reduction in VDW adhesion could not be attributed to a reduction in the spine (echini) tip radii upon organic pyrolysis. Indeed, the hematite and magnetite replicas containing different amounts of iron oxide, and exhibiting different degrees of firing shrinkage, exhibited similar VDW adhesion force values. Application of a simple Hamaker model indicated that the VDW adhesion of these oxide replicas was consistent with the contact of fine oxide nanocrystals located on the spine tips (and not the curvature of the overall spine tip itself) with underlying surfaces.

The Fe_3O_4 pollen replicas exhibited significant longer-range attraction (out to 1.5 mm) to a magnetic substrate, with the magnetic force increasing monotonically with an increase in the oxide content of the replica microparticles. Indeed, the total force (VDW + magnetic) of attraction to the magnetic substrate

was 56% greater for the Fe₃O₄ pollen replicas prepared with 50 SSG cycles than for the native cleaned sunflower pollen. A simple model was developed that, with knowledge of the magnetization of the Fe₃O₄ pollen replica, the Fe₃O₄ content of the replica, and the simulated field gradient of the magnetic substrate, provided a good description of the magnetic force of attraction as a function of distance from the magnetic substrate.

The conformal coating-based replication process, coupled with the models for VDW and magnetic attraction developed in this work, may be applied to a variety of hydroxyl-bearing micro-particles of biogenic or synthetic origin to generate 3-D magnetic oxide replicas with predictable and tailorable multi-modal adhesion.

Acknowledgements

This work was supported by the U.S. Air Force Office of Scientific Research via Award no. FA9550-10-1-0555.

Notes and references

- 1 J. de Vicente, D. J. Klingenberg and R. Hidalgo-Alvarez, *Soft Matter*, 2011, **7**, 3701; K. Nandy, S. Chaudhuri, R. Ganguly and I. K. Puri, *J. Magn. Magn. Mater.*, 2008, **320**, 1398; S. Rudge, C. Peterson, C. Vessely, J. Koda, S. Stevens and L. Catterall, *J. Controlled Release*, 2001, **74**, 335; A. S. Wadajkar, S. Santimano, L. Tang and K. T. Nguyen, *Biomaterials*, 2014, **35**, 654; C. Gosse and V. Croquette, *Biophys. J.*, 2002, **82**, 3314; A. Rida and M. A. M. Gijs, *Anal. Chem.*, 2004, **76**, 6239; J. C. Love, A. R. Urbach, M. G. Prentiss and G. M. Whitesides, *J. Am. Chem. Soc.*, 2003, **125**, 12696; W. Wen, N. Wang, D. W. Zheng, C. Chen and K. N. Tu, *J. Mater. Res.*, 1999, **14**, 1186; R. M. Erb, R. Libanori, N. Rothfuchs and A. R. Studart, *Science*, 2012, **335**, 199.
- 2 F. E. Round, R. M. Crawford and D. G. Mann, *The Diatoms: Biology and Morphology of the Genera*, Cambridge University Press, New York, 1990; D. M. Nelson, P. Treguer, M. A. Brzezinski and A. Leynaert, *Global Biogeochem. Cycles*, 1995, **9**, 359; D. G. Mann and S. J. M. Droop, *Hydrobiologia*, 1996, **336**, 19; M. Hildebrand, *Chem. Rev.*, 2008, **108**, 4855; N. Kroger and N. Poulsen, *Annu. Rev. Genet.*, 2008, **42**, 83.
- 3 G. O. W. Kremp, *Morphologic Encyclopedia of Palynology*, University of Arizona Press, Tucson, AZ, USA, 2nd edn, 1968; J. W. Walker and J. A. Doyle, *Ann. Mo. Bot. Gard.*, 1975, **62**, 664; G. Erdtman and E. J. Brill, *Pollen Morphology and Plant Taxonomy*, Leiden, The Netherlands, 1986; A. Ressayre, B. Godelle, C. Raquin and P. H. Gouyon, *J. Exp. Zool.*, 2002, **294**, 122; P. J. Beggs, *Clin. Exp. Allergy*, 2004, **34**, 1507; L. Ziska, K. Knowlton, C. Rogers, D. Dalan, N. Tierney, M. A. Elder, W. Filley, J. Shropshire, L. B. Ford, C. Hedberg, P. Fleetwood, K. T. Hovanky, T. Kavanaugh, G. Fulford, R. F. Vrtis, J. A. Patz, J. Portnoy, F. Coates, L. Bielory and D. Frenz, *Proc. Natl. Acad. Sci. U. S. A.*, 2011, **108**, 4248; W. Songnuan, *Asian Pac. J. Allergy Immunol.*, 2013, **31**, 261.
- 4 R. Wetherbee, J. L. Lind, J. Burke and R. S. Quatrano, *J. Phycol.*, 1998, **34**, 9; K. S. Kopanska, B. Tesson, H. Lin, J. C. Meredith, M. Hildebrand and A. Davis, *Silicon*, 2014, **6**, 95; A. F. Edlund, R. Sqanson and D. Preuss, *Plant Cell*, 2004, **16**, S84.
- 5 K. H. Sandhage, M. B. Dickerson, P. M. Huseman, M. A. Caranna, J. D. Clifton, T. A. Bull, T. J. Heibel, W. R. Overton and M. E. A. Schoenwaelder, *Adv. Mater.*, 2002, **14**, 429; S. R. Hall, H. Bolger and S. Mann, *Chem. Commun.*, 2003, 2784; C. S. Gaddis and K. H. Sandhage, *J. Mater. Res.*, 2004, **19**, 2541; J. Zhao, C. S. Gaddis, Y. Cai and K. H. Sandhage, *J. Mater. Res.*, 2005, **20**, 282; Y. Wang, Z. Liu, B. Han, Z. Sun, J. Du, J. Zhang, T. Jiang, W. Wu and Z. Miao, *Chem. Commun.*, 2005, 2948; Y. Cai, S. M. Allan, F. M. Zalar and K. H. Sandhage, *J. Am. Ceram. Soc.*, 2005, **88**, 2005; S. Shian, Y. Cai, M. R. Weatherspoon, S. M. Allan and K. H. Sandhage, *J. Am. Ceram. Soc.*, 2006, **89**, 694; S. R. Hall, V. M. Swinerd, F. N. Newby, A. M. Collins and S. Mann, *Chem. Mater.*, 2006, **18**, 598; U. Kusari, Z. Bao, Y. Cai, G. Ahmad, K. H. Sandhage and L. G. Sneddon, *Chem. Commun.*, 2007, 1177–1179; S.-J. Lee, S. Shian, Ch.-H. Huang and K. H. Sandhage, *J. Am. Ceram. Soc.*, 2007, **90**, 1632; Y. Fang, V. W. Chen, Y. Cai, J. D. Berrigan, S. R. Marder, J. W. Perry and K. H. Sandhage, *Adv. Funct. Mater.*, 2012, **22**, 2550; Y. Xia, W. Zhang, Z. Xiao, H. Huang, H. Zeng, X. Chen, F. Chen, Y. Gan and X. Tao, *J. Mater. Chem.*, 2012, **22**, 9209.
- 6 W. B. Goodwin, I. J. Gomez, Y. Fang, J. C. Meredith and K. H. Sandhage, *Chem. Mater.*, 2013, **25**, 4529.
- 7 H. E. M. Dobson, *Am. J. Bot.*, 1988, **75**, 170.
- 8 M. R. Weatherspoon, Y. Cai, M. Crne, M. Srinivasarao and K. H. Sandhage, *Angew. Chem., Int. Ed.*, 2008, **47**, 7921; M. R. Weatherspoon, M. B. Dickerson, G. Wang, Y. Cai, S. Shian, S. C. Jones, S. R. Marder and K. H. Sandhage, *Angew. Chem., Int. Ed.*, 2007, **46**, 5724; G. Wang, Y. Fang, P. Kim, A. Hayek, M. R. Weatherspoon, J. W. Perry, K. H. Sandhage, S. R. Marder and S. C. Jones, *Adv. Funct. Mater.*, 2009, **19**, 2768; J. P. Vernon, N. Hobbs, Y. Cai, A. Lethbridge, P. Vukusic, D. D. Deheyn and K. H. Sandhage, *J. Mater. Chem.*, 2012, **22**, 10435; J. P. Vernon, Y. Fang, Y. Cai and K. H. Sandhage, *Angew. Chem., Int. Ed.*, 2010, **49**, 7765.
- 9 F. N. Rhines, W. A. Johnson and W. A. Anderson, *Trans. Metall. Soc. AIME*, 1942, **147**, 205.
- 10 *Principles of Electricity and Magnetism*, ed. E. M. Pugh and E. W. Pugh, Addison-Wesley, Reading, MA, 1960; *Electricity and Magnetism*, ed. M. H. Nayfeh and M. K. Brussel, John Wiley, New York, 1985.
- 11 N. Leventis and X. Gao, *Anal. Chem.*, 2001, **73**, 3981.
- 12 E. Dominquez, J. A. Mercado, M. A. Quesada and A. Heredia, *Sex. Plant Reprod.*, 1999, **12**, 171.
- 13 I. Ichinose, H. Senzu and T. Kunitake, *Chem. Lett.*, 1996, 831; I. Ichinose, H. Senzu and T. Kunitake, *Chem. Mater.*, 1997, **9**, 1296.
- 14 H. A. Wriedt, *J. Phase Equilib.*, 1991, **12**, 170.

- 15 Card No. 33-0664 for α -Fe₂O₃, Card No. 19-0629 for Fe₃O₄; International Center for Diffraction Data: Newtown Square, PA USA, 2007.
- 16 K. Tanaka, T. Yoko, M. Atarashi and K. Kamiya, *J. Mater. Sci. Lett.*, 1989, **8**, 83; J. Tang, K.-Y. Wang and W. Zhou, *J. Appl. Phys.*, 2001, **89**, 7690; S. Chatman, A. J. G. Noel and K. M. Poduska, *J. Appl. Phys.*, 2005, **98**, 113902; M. Sanz, M. Oujja, E. Rebollar, J. F. Marco, J. de la Figuera, M. Monti, A. Bollero, J. Camarero, F. J. Pedrosa, M. Garcia-Hernandez and M. Castillejo, *Appl. Surf. Sci.*, 2013, **282**, 642.
- 17 J. C. Meredith, A. P. Smith, A. Karim and E. J. Amis, *Macromolecules*, 2000, **33**, 9747.
- 18 H. C. Hamaker, *Physica*, 1937, **4**, 1058.
- 19 *Intermolecular and Surface Forces*, ed. J. Israelachvili, Academic Press, London, 1992.
- 20 J. L. Rosenholtz and D. T. Smith, *Am. Mineral.*, 1936, **21**, 115; H. Daoust and M. Rinfret, *J. Colloid Sci.*, 1952, **7**, 11; M.-H. Chiu, J.-Y. Lee and D.-C. Su, *Appl. Opt.*, 1999, **38**, 4047; C. U. Devi, A. K. Sharma and V. V. R. N. Rao, *Mater. Lett.*, 2002, **56**, 167; R. J. Nussbaumer, W. R. Caseri, P. Smith and T. Tervoort, *Macromol. Mater. Eng.*, 2003, **288**, 44; *CRC Handbook of Chemistry and Physics*, ed. D. R. Lide, CRC Press, Boca Raton, FL, 2005, Internet Version, <http://www.hbcpnetbase.com>; S. L. Atkin, S. Barrier, Z. Cui, P. D. I. Fletcher, G. Mackenzie, V. Panel, V. Sol and X. Zhang, *J. Photochem. Photobiol., B*, 2011, **102**, 209.